Determination of polar stratospheric cloud particle refractive indices by use of *in situ* optical measurements and *T*-matrix calculations

Claudio Scarchilli, Alberto Adriani, Francesco Cairo, Guido Di Donfrancesco, Carlo Buontempo, Marcel Snels, Maria Luisa Moriconi, Terry Deshler, Niels Larsen, Beiping Luo, Konrad Mauersberger, Joelle Ovarlez, Jim Rosen, and Jochen Schreiner

A new algorithm to infer structural parameters such as refractive index and asphericity of cloud particles has been developed by use of *in situ* observations taken by a laser backscattersonde and an optical particle counter during balloon stratospheric flights. All three main particles, liquid, ice, and a no-ice solid (NAT, nitric acid trihydrate) of polar stratospheric clouds, were observed during two winter flights performed from Kiruna, Sweden. The technique is based on use of the *T*-matrix code developed for aspherical particles to calculate the backscattering coefficient and particle depolarizing properties on the basis of size distribution and concentration measurements. The results of the calculations are compared with observations to estimated refractive indices and particle asphericity. The method has also been used in cases when the liquid and solid phases coexist with comparable influence on the optical behavior of the cloud to estimate refractive indices. The main results prove that the index of refraction for NAT particles is in the range of 1.37–1.45 at 532 nm. Such particles would be slightly prolate spheroids. The calculated refractive indices for liquid and ice particles are 1.51–1.55 and 1.31–1.33, respectively. The results for solid particles confirm previous measurements taken in Antarctica during 1992 and obtained by a comparison of lidar and optical particle counter data.

OCIS codes: 010.0010, 290.3030, 290.5850, 010.1110, 290.5820.

1. Introduction

During the winter the polar stratosphere radiatively cools enough to allow for the formation of clouds. These polar stratospheric clouds (PSCs) are the most important forerunners for ozone depletion processes.[1] The heterogeneous chemical reactions on or within PSC particles convert relatively unreactive chlorine and bromine compounds into reactive species that enter into ozone-destroying catalytic cycles. Also, sedimentation of large PSC particles that contain nitric acid causes denitrification, which leads to increased ozone loss.[2] The chemical reactions that lead to ozone destruction, as well as the PSC potential for dehydration and denitrification of the polar stratosphere, are linked to the compositions, thermodynamic phase, and dimensions of their particles.

Optical parameters, such as depolarization and backscatter ratio, accessible from lidar sounding

C. Scarchilli, F. Cairo, C. Buontempo, M. Snels, and M. L. Moriconi are with the Institute of Atmospheric Sciences and Climate, Italian National Research Council, Via Fosso del Cavaliere, 100-00133 Rome, Italy. A. Adriani (adriani@atmos.ifa.rm.cnr.it) is with the Institute for Interplanetary Space Physics, Istituto Nazionale di Astrofisica, Rome, Italy. G. Di Donfrancesco, as well as C. Scarchilli, is with the Ente per le Nuove Technologie l'Energia el'Ambiente, Sezione Clima, Via Anguillarese 301, 00060 Santa Maria di Galeria, Rome, Italy. T. Deshler and J. Rosen are with the Department of Atmospheric Science, College of Engineering, University of Wyoming, 1000 East University Avenue, Laramie, Wyoming 82071. N. Larsen is with the Danish Meteorological Institute, Division of Middle Atmosphere Research, Lyngbyvej 100, 2100 Copenhagen, Denmark. B. Luo is with the Institute for Atmospheric and Climate Science, Swiss Federal Institute of Technology, Schafmattstrasse 30, CH-8093 Zurich, Switzerland. K. Mauersberger and J. Schreiner are with the Max-Planck-Institut für Kernphysik, Saupfercheckweg 1, D-69117 Heidelberg, Germany. J. Ovarlez is with the Laboratoire de Meteorologie Dynamique, Ecole Polytechnique, Centre National de la Recherche Scientifique, 91128 Palaiseau Cedex, France.

Received 19 March 2004; revised manuscript received 29 September 2004; accepted 7 October 2004.

0003-6935/05/163302-10$15.00/0

studies,[3] have been used to classify different categories of PSC. The backscatter ratio, defined as the ratio between the lidar return and the estimation of the backscattered return that is due to a particle-free atmosphere, detects and quantifies the presence of optically active particles in an air mass. The lidar lasers usually have a polarized emission, then the value of depolarization ratio, defined as the ratio between the perpendicular backscattered return divided by the parallel backscattered return, is related to the shape of the particles. For spherical particles, such as liquid droplets, this ratio is zero, but an enhancement of depolarization can arise from scattering of nonspherical particles, such as solid ones. Based on these observations, three main categories of PSCs were identified[4]: solid nitric acid trihydrate (NAT), showing a low backscatter ratio and high depolarization, liquid, showing a high backscatter ratio and low depolarization, and ice, with both high depolarization and backscatter ratio. Both theoretical and experimental studies identified liquid PSC particles as formed by ternary solutions of $H_2O/HNO_3/H_2SO_4$ (Refs. 5–7) and solid NAT PSC particles as solid hydrates of nitric acid.[8–11] Quantitative information on PSC particle properties can be derived from lidar studies once a suitable optical modeling of the studied particles is used.

The theory that describes optical scattering for spherical particles was developed by Mie in the early 1900s. During the latter 1900s more computational capability and newly developed mathematical tools, the T matrix,[12] became available to describe the scattering of arbitrarily shaped particles. Here we apply the T-matrix theory to compare *in situ* measurements of particle size distribution and optical scattering. Values of aspect ratio and index of refraction, which minimize the difference between measured and modeled optical scattering, describe the phase and composition of the particles measured.

2. Mathematical Tools

The polarization state of a beam of light is traditionally described by a vector $\mathbf{I} = (I, Q, U, V)^T$ composed of four Stokes parameters. The first Stokes parameter, I, is the intensity, whereas the other three parameters describe the polarization state of the beam and those parameters can be described as a linear combination of the electromagnetic field components and their complex conjugate[13]:

$$\begin{aligned} I &= E_\theta E_\theta^* + E_\varphi E_\varphi^*, \qquad U = -E_\theta E_\varphi^* - E_\varphi E_\theta^* \\ Q &= E_\theta E_\theta^* - E_\varphi E_\varphi^*, \qquad V = i(E_\varphi E_\theta^* - E_\theta E_\varphi^*). \end{aligned} \tag{1}$$

The scattering of a beam of light by a single particle or a collection of particles can be described in matrix form as $\mathbf{I}^{sca} = \mathbf{F}\mathbf{I}^{inc}$, where the 4×4 matrix $\mathbf{F}$, known as the Mueller matrix, describes the transformation of the Stokes vector of the incident beam into the Stokes vector of the beam scattered toward a particular direction. In general, electromagnetic scattering produces light with polarization characteristics different from those of an incident beam.

When considering single scattering by a small-volume element composed of a collection of sparsely distributed, randomly oriented and nonabsorbing scattering particles, the Mueller matrix has the well-known, simplified block-diagonal structure[14]

$$F(\Theta) = \begin{bmatrix} F_{11}(\Theta) & F_{12}(\Theta) & 0 & 0 \\ F_{12}(\Theta) & F_{22}(\Theta) & 0 & 0 \\ 0 & 0 & F_{33}(\Theta) & F_{34}(\Theta) \\ 0 & 0 & -F_{34}(\Theta) & F_{44}(\Theta) \end{bmatrix} \tag{2}$$

with only six independent matrix elements and where Θ is the scattering angle. In the exact backscattering ($\Theta = \pi$) direction F became diagonal and has only two independent elements:

$$F(\pi) = [F_{11}(\pi),\ F_{22}(\pi),\ -F_{22}(\pi),\ F_{11}(\pi) - 2F_{22}(\pi)]. \tag{3}$$

If we assume that the incident beam is linearly polarized and parallel to the scattering plane such that its Stokes vector assumes the form (1,1,0,0), then the linear depolarization ratio, defined as the ratio of the flux of the cross-polarized component of the backscattered light relative to that of the copolarized component, can be written as[15]

$$\frac{\mathbf{F}_{11}(\pi) - \mathbf{F}_{22}(\pi)}{\mathbf{F}_{11}(\pi) + \mathbf{F}_{22}(\pi)} = \delta^p. \tag{4}$$

In general, the second Stokes parameter of the light backscattered by a generic particle is not equal to the first Stokes parameter. Only for the particular case of backscattering by a spherical particle is F_{11} equal to F_{22} and the depolarization ratio is 0.

The T-matrix method[16] resolves the problem of computing the F-matrix elements for scattering produced by generic rotationally symmetric particles. The linearity of Maxwell's equations implies that the coefficients of the scattered field are linearly related to those of the incident field. The linear transformation that connects these two sets of coefficients is called the T (for transition) matrix. The elements of T are independent of incident and scattering fields, but they do depend on refractive index, shape (aspect ratio), and orientation of the particle.

A suitable software based on the T-matrix approach, developed from the original work of Mishchenko and Travis[17], is used to calculate the single-particle backscattering cross section ($\mathbf{C}_{sca}$) and the elements of the scattering matrix (F) for spheroidal particles randomly oriented, as a function of their aspect ratio (AR), refractive index (RI), size parameter ($r^{TM} = R^{TM}/\lambda$, where R^{TM} is the volume equivalent sphere radius, and λ is the wavelength of the light involved in the scattering process), and scattering angle (Θ).[17] We created a database of $\mathbf{C}_{sca}$ by varying the AR from 0.50 to 2.00 (from an oblate to a prolate

spheroid) in steps of 0.05, the RI ranges from 1.31 to 1.59 in steps of 0.02, and finally r^{TM} ranges from 0.1 to 25 in steps of 0.01. For extreme ARs, the computational code did not converge. Thus in such cases $\mathbf{C}_{sca}$ has been extrapolated from the closest converging ones. The extrapolation was based on a scaling proportional to the square of an equivalent particle surface.

From the backscattering cross section, it is easy to obtain the aerosol backscattering coefficient given by

$$\beta_M^p = \int N(R) \cdot \mathbf{C}_{sca}(R^{TM}) \cdot \mathbf{F}_{11}(\pi) dR \tag{5}$$

for a collection of scatterers with volume number density N. Subscript M represents parameter values computed by model calculations. β^p, as well as the aerosol depolarization, is the parameter that is accessible through experimental investigation.

3. Instrumentation and Data

The research presented here is based on a series of time measurements taken with optical particle counters (OPCs)[18] and backscattersondes[19–21] while traversing PSC layers; the performance and dataset of these instruments are briefly described below.

A. Optical Particle Counter

The OPC measures and sizes the concentration of optically detectable aerosol particles with radii R ranging from 0.01 to greater than 10 μm, which, according to their dimensions, are divided into twelve size classes defined by suitable values of limiting radii R_j (j = 0–12). The actual values of R_j are slightly dependent on the index of refraction hypothesized when processing OPC raw data. Variations in radius bin widths $\Delta r_j = R_j - R_{j+1}$ up to 8% can occur for particles with a RI ranging from 1.29 to 1.61. The size of the particles is calculated from the intensity of white light scattered at 40° with respect to the forward direction by use of the Mie theory for spherical particles.[18] This value of the scattered angle has been chosen to ensure a monotonic relationship between scattered light and particle size bins for spherical particles.

The uncertainty in measured concentrations N_j of particles with a radius in a defined size bin is due to counting statistics and is defined as $\sigma = (N_j N_{min})^{1/2}$, where N_{min} is the minimum concentration measurable with these instruments, estimated to be of the order of 10^{-4} particles cm^{-3}. The dataset of this instrument is composed of a time series of 10-s particle size spectra through PSCs. Thus, for each OPC measurement we obtained sets of 13 differential concentrations $N_j(RI, t)$ of particles with radii within the jth radius bin, defined as the number density of particles with a radius between R_j and R_{j+1}. The bin widths, as mentioned above, are slightly dependent on the particular choice of index of refraction that we used to process the raw data.

B. Backscattersondes

The laser backscattersonde (LABS) is based on the use of microlasers. The LABS partially uses lidar technology but does not require high laser power and long ranges, and it is an instrument created for *in situ* measurements. In fact, the light backscattered from the atmosphere that reaches the collecting optics comes from a range of 5–40 m (approximately 90% of the signal actually comes from the closest 20 m). The instrument is equipped with two lasers at 532- and 685-nm wavelength. The laser light has an on–off modulation to provide sky background measurements. The detectors used are photomultipliers that work in the photon-counting mode. The LABS has a relatively low power consumption and is small in size.

Atmospheric optical parameters retrieved from the instrument's data are the volume backscatter ratio

$$R^{vol}(t) = \frac{\beta^p(t) + \beta^{mol}(t)}{\beta^{mol}(t)} = 1 + R^p, \tag{6}$$

where β^p, β^{mol}, and R^p are, respectively, the aerosol and molecular backscattering coefficients and the aerosol backscatter ratio. The uncertainty of this parameter is estimated to be less than 5%. When we use Eq. (5) the aerosol backscatter coefficient is

$$\beta^p(t)_{experimental} = R^p(t) * \beta^{mol}(t), \tag{7}$$

where

$$\beta^{mol}(t) = K(\lambda) * \frac{P(t)}{T(t)} \tag{8}$$

is the molecular backscatter coefficient calculated from atmospheric pressure P, temperature T as measured by the sensors of the balloon payload, λ is the wavelength of incident light, and K is a function that depends on wavelength. Moreover, since the backscattered signal is split into parallel and cross-polarized components and then detected, the instrument also allows assessment of the volume depolarization ratio

$$\delta = \frac{\beta_{orthogonal}{}^p + \beta_{orthogonal}{}^{mol}}{\beta_{parallel}{}^p + \beta_{parallel}{}^{mol}} \tag{9}$$

as the ratio between the signals detected in two channels, normalized such that it attains the value of 0.014, corresponding to molecular depolarization, in regions of the atmosphere presumed to be free of aerosols.[22] From the volume depolarization, the aerosol depolarization

$$\delta^p = \frac{\beta_{orthogonal}{}^p}{\beta_{parallel}{}^p} \tag{10}$$

is easily obtainable[22] when aerosols are present in the air masses.

4. Method

The scope of our research is to compare the backscatter coefficients and depolarization measured by the LABS with the same parameters as computed by optical modeling. These latter quantities are computed from the scatter size distribution spectra experimentally retrieved from the size distribution spectra measured with an OPC. The best match between experimentally measured and theoretically computed optical parameters will be obtained for one given particle refractive index and aspect ratio. In this way, the mean particle refractive index and shape can be assessed given optical and size-resolved particle measurements. Often the measured size particle distributions are presented by fitting them by use of a monomodal or bimodal log-normal function. For this paper we decided to use observed data without a log-normal approximation mainly for the following reasons. First, it is more straightforward to use direct measurements than products of elaboration, since large differences in the results were not expected. Second, it was easier to define constraints on the optical parameters for calculations starting with the uncertainties of the measurements rather than with the degree of likelihood of the fitted log-normal parameters. Third, the use of further products of elaboration as the log-normal size distribution can introduce uncertainties that are due to the approximation process more than to the variability of the experimental parameters.

Computation of the modeled optical parameters has been performed under the assumption that the particle size spectra is well represented by histograms provided by the OPC data. Taking into account the uncertainties associated with each OPC measurement, two histograms for each measurement have been considered in the computation. One, representing the upper limit for the size distribution, has been created by incrementing the particle density value by the measurement uncertainty for each radius bin. The other, representing the lower limit, has been created by decrementing these densities by the same amount. This amount is equal to the estimated instrumental error on the concentration measurements. The measured size distribution is slightly dependent on the refractive index of the particles. The original size distribution has been given for a refractive index of 1.45. Then a correction of the bin sizes was needed for any calculation with a new refractive index.[18] These two size spectra histograms from a single measurement, used once in the optical modeling, give pairs of computed optical parameters. These pairs, namely,

$$\left[\beta_M{}^p(\mathrm{RI},\ \mathrm{AR},\ t)\right]^{\max},\ \left[\beta_M{}^p(\mathrm{RI},\ \mathrm{AR},\ t)\right]^{\min},$$
$$\left[\delta_M{}^p(\mathrm{RI},\ \mathrm{AR},\ t)\right]^{\max},\ \left[\delta_M{}^p(\mathrm{RI},\ \mathrm{AR},\ t)\right]^{\min},$$

define the interval of values into which the optical measurements must fit. However, the computed minimum-to-maximum range for depolarization was sensitively lower than the one given by the experimental error. Then a new range was set taking into account the estimated experimental error of 0.015.

Finally, we searched for the values of the AR and the RI that fulfill the inequalities at each time t:

$$\left[\beta_M{}^p(\mathrm{RI},\ \mathrm{AR},\ t)\right]^{\min} \le \left[\beta_{\mathrm{experimental}}{}^p(t)\right] \le \left[\beta_M{}^p(\mathrm{RI},\ \mathrm{AR},\ t)\right]^{\max} \quad (11)$$

for the backscatter coefficient and

$$\left[\delta_M{}^p(\mathrm{AR},\ \mathrm{AR},\ t)\right] - 1.5 \le \left[\delta_{\mathrm{experimental}}{}^p(t)\right] \le \left[\delta_M{}^p(\mathrm{AR},\ \mathrm{RI},\ t)\right] + 1.5(\%). \quad (12)$$

5. Data Comparison

A. Flight of 25 January 2000

The balloon was launched on 25 January 2000 from Esrange near Kiruna, Sweden. It reached its floating altitude at 24 km and ascended and descended three times between 20 and 24 km. The PSC was met at 74900 UT; the cloud extended horizontally for more than 200 km, and it was observed between 20 and 24 km for more than 2 h. Here only the first part of the flight is considered for calculations because not all the optical data were available during the second part of the flight. During the initial ascent we measured temperatures of 1–2 K below the frost point, increasing to near T_{NAT} during the latter part of the flight.

Figure 1(a) shows the subset 74900–76200 UT of the complete time series of the observations the aerosol depolarization, the backscatter coefficient at 532 nm, and the measured temperature. Figure 1(b) shows the same time sequence of differential concentration density. The small boxes in Fig. 1 show the size distributions at two different times as histograms.

The time series was divided into five subintervals in which optical parameters, mixing ratios, and concentrations of the PSC could be considered sufficiently self-consistent and the parameters can be averaged over time to give values representative of the different cloud layers. As can be seen in the $L1$ and $L2$ subinterval, PSC particles can be considered as liquid because of their low depolarization values. This corresponds to the high density of small particles ($r < 1\ \mu\mathrm{m}$) and to the low density of large particles. On the other hand, in $S1$ and $S2$ high depolarization values and density of large particles suggest that these particles are solid. Finally, in the T subinterval the high variability of the parameters suggests a mixed phase cloud. Figure 2 shows the average particle size distributions and values of volume and aerosol depolarization for each subinterval.

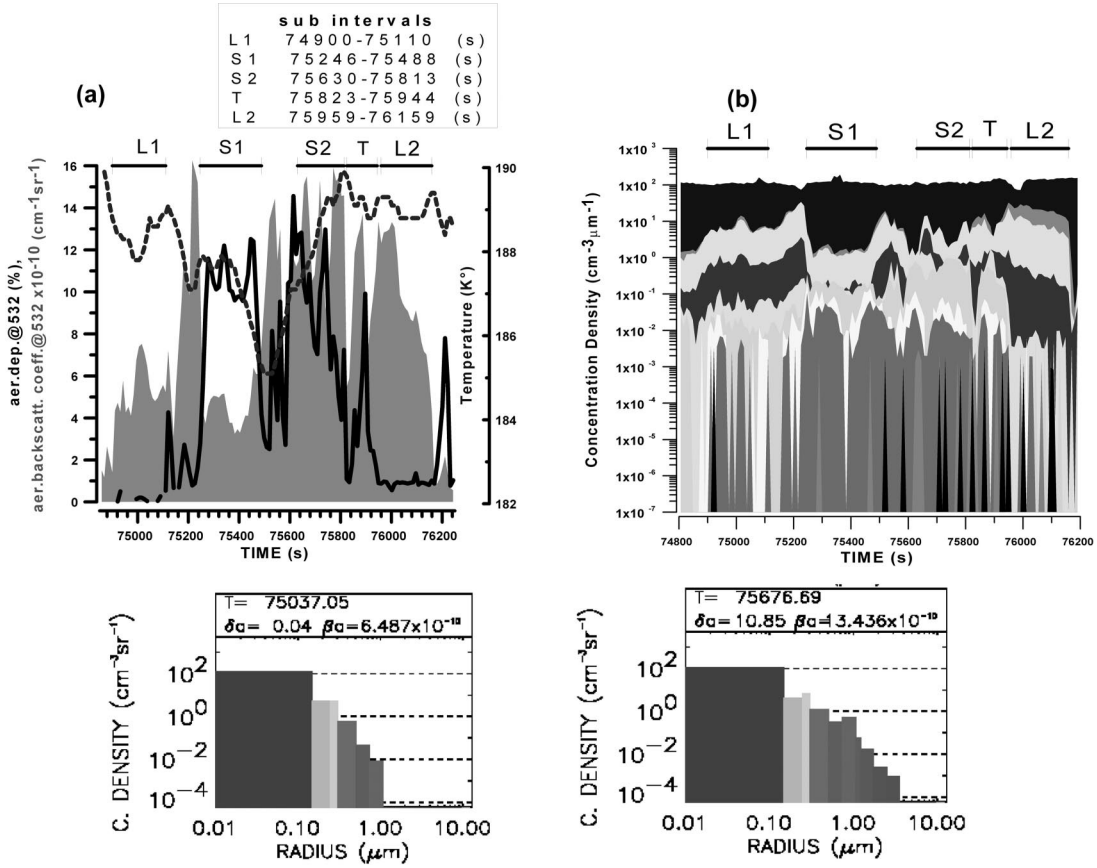

Fig. 1. (a) Kiruna, 25 January 2000. Time series of aerosol depolarization (black), aerosol backscatter coefficient (gray) at 532 nm, and temperature (dashed gray). The legend gives the time intervals considered in the calculations. (b) Time series of concentration density in each bin at an index of refraction of 1.45. Gray scale colors represent different radius bins: 0.01–0.15, 0.15–0.25, 0.25–0.30, 0.30–0.50, 0.50–0.75, 0.75–1.08, 1.08–1.25, 1.25–1.75, 1.75–2.50, and 2.50–3.50 μm. Small boxes: particulars of concentration densities as a function of particle radius at time T, color bins are the same as in (b). Values of $\delta^{\text{experimental}}$ and $\beta^{\text{experimental}}$ are signed for two different times.

We calculated the optical characteristics of PSC particle distributions ($[\beta_M{}^p(\mathrm{RI}, \mathrm{AR}, t)]$, $[\delta_M{}^p(\mathrm{AR}, \mathrm{RI}, t)]$) by using the T-matrix algorithm for each measurement. These sets of values were averaged over the five subintervals, and we applied the two inequalities, (11) and (12), to determine the pairs of AR and RI that simultaneously fulfill them. The results of the comparison are shown in Fig. 3. For $L1$ and $L2$ a high value of index of refraction was found ranging from 1.53 to 1.55; all the solutions for inequality (12) give a value of aspect ratio close to 1 corresponding to approximately spherical particles. For $S1$ and $S2$ the index of refraction can vary from 1.35 to 1.45 and the AR value is approximately equal to 1.05, which corresponds to slightly prolate spheroid solid particles. Finally in a T subinterval there is no solution for the system perhaps because of sampling a mixed phase cloud.

Calculations to determine refractive indices for each single point in the subintervals have also been performed to verify if the distribution of the results was consistent with the average values found previously. In Fig. 4 we plotted the values of refractive index RI calculated for the single data points of the cloud (Fig. 1) versus aerosol depolarization δ_p. Different gray colors are related to different time subintervals. Two well-defined zones are observed. The first is characterized by high depolarization and a low-to-medium refractive index, which are NAT particles.[11] The second zone, with low depolarization and a high

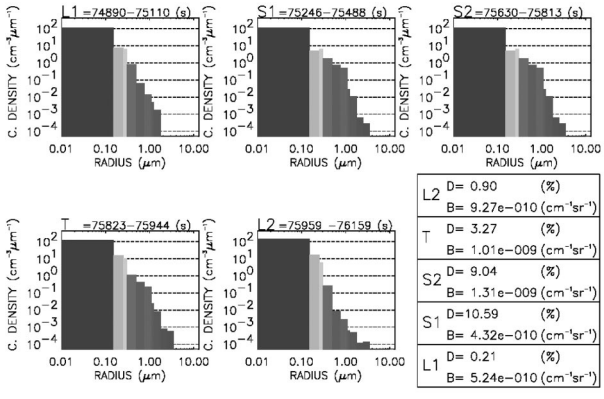

Fig. 2. Average distribution concentration density versus radius for the five subintervals of interest. The legend lists the average values of aerosol depolarization and backscatter coefficient at 532 nm for each subinterval.

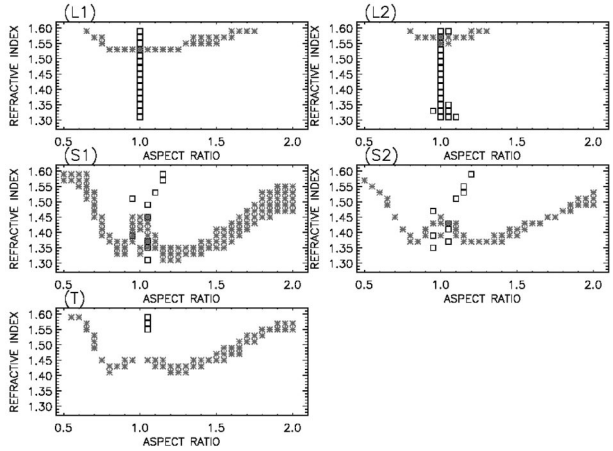

Fig. 3. Kiruna, 25 January 2000. For each subinterval, the crosses represent pairs of RI and AR that fulfill the backscatter coefficient inequality (11); see text. Open squares represent pairs of RI and AR that satisfy inequality (12); see text. Values of RI and AR that simultaneously fulfill the imposed conditions can easily be discerned from these graphs and are placed at the intersection of the two curves.

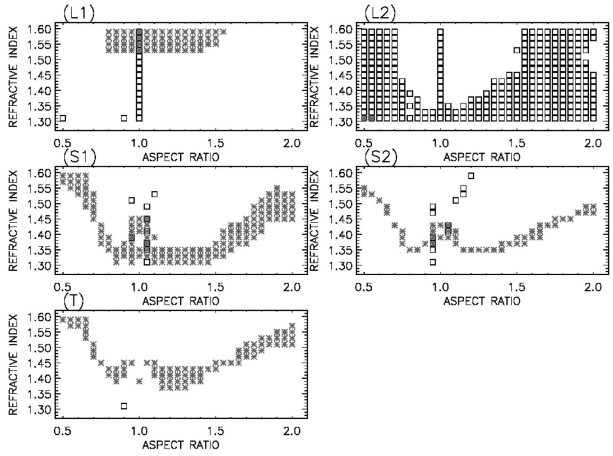

Fig. 5. Kiruna, 25 January 2000. Particle distribution is formed by particles with $R < 0.56$ μm in the liquid phase and particles with $R > 0.56$ μm in the solid phase. For each subinterval the crosses represent pairs of RI and AR that fulfill the backscatter coefficient inequality (11). Open squares represent pairs of RI and AR that satisfy inequality (12) for solid particles.

refractive index, is formed by nondepolarizing liquid particles [i.e., supercooled ternary solution (STS)].

Recent studies[23] have pointed out that PSCs can seldom exist in a mixed state in which liquid particles can coexist, not in thermodynamic equilibrium but nevertheless not for long times, with fewer solid particles in a growing or evaporating stage. Such a situation can also be encountered in the T subinterval. Model studies suggest that in such cases the solid particles grow bigger than the liquid particles that remain smaller.[24] To reproduce such a mixed phase PSC, we thus changed the way to model the size distribution and defined a cutoff radius in such a way that particles with a radius smaller than the cutoff are considered to be in the liquid phase, and particles with a radius greater than the cutoff radius are considered solid. Then AR 1 and RI 1.53 of the particles, below the cutoff radius were fixed, leaving the RI and degree of asphericity of the particles above the cutoff radius as unknowns.

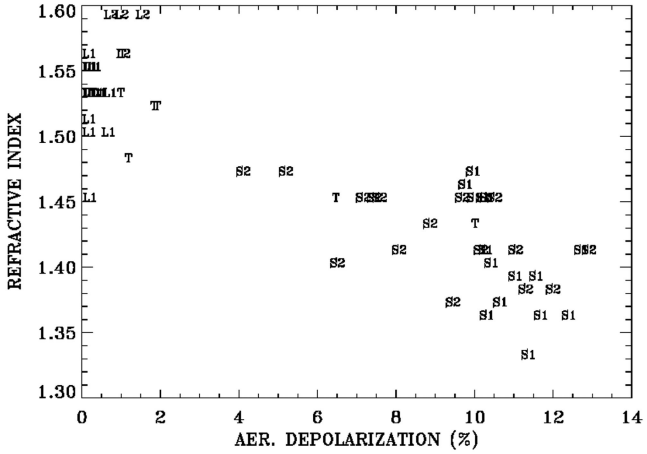

Fig. 4. Values of index of refraction versus depolarization aerosol. Different gray colors are related to different time subintervals. Transparent points belong to no subintervals.

The values of $[\beta_M^p(\mathrm{RI}, \mathrm{AR}, t)]$ and $[\delta_M^p(\mathrm{AR}, \mathrm{RI}, t)]$ that fulfilled inequalities (11) and (12) were calculated when the cutoff radius AR and RI of the particles varied. Different cutoffs have been tested among the radius values that divide two adjacent bins (0.28, 0.56, 0.8, and 1.02 μm) once the refractive index of the liquid part was fixed to 1.53 in the 0.1–1.1-μm range. The best cutoff radius that gave the most acceptable physical results was equal to 0.56 μm. Indirect evidence of the accuracy of such a result came from microphysical modeling of this PSC event when modeled size distributions showed the onset of solid particles at a radius close to our findings.

The comparison between the experimental data and the optical parameter calculated with the new model is depicted in Fig. 5 where, for each subinterval, the crosses represent pairs of RI and AR that fulfill the backscatter coefficient inequality (11), and the open squares represent pairs of RI and AR that satisfy inequality (12). The results are quite similar to the above results. In subintervals $L1$ and $L2$ the particle distribution is composed of small spherical particles with the indices of refraction ranging between 1.53 and 1.6. For subinterval T, in which the presence of mixed state particles was assumed, the new model finds values of AR = 0.9 and RI = 1.33 on the depolarization curve, in contrast with the results shown in Fig. 3. In the T interval, the values of AR and RI are in agreement with the ones previously reported for subintervals $S1$ and $S2$.

It is also of interest to study how this new model tackles the $S1$ and $S2$ subintervals. In the $S1$ and $S2$ intervals, where particles below the cutoff radius in the size distribution are assumed to be liquid, the algorithm still reproduces results for AR and RI con-

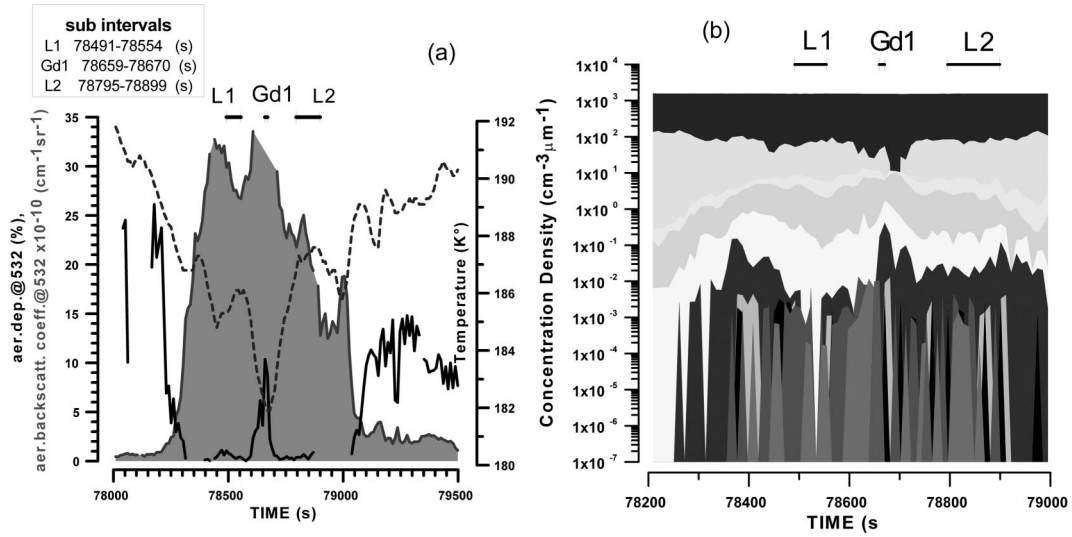

Fig. 6. (a) Kiruna, 9 December 2001. Time series, from 78400 to 78900 UT, of aerosol depolarization (black) and backscatter aerosol coefficient (gray) at 532 nm, temperature measured with a LABS (dashed black). The legend lists the time intervals considered in the calculations. (b) Particle concentration time series from 78400 to 78900 UT in each bin at an index of refraction of 1.45. The gray scale represents different radius bins: 0.01–0.15, 0.15–0.25, 0.25–0.30, 0.30–0.50, 0.50–0.75, 0.75–1.08, 1.08–1.25, 1.25–1.75, 1.75–2.50, and 2.50–3.50 μm.

sistent with the above study when no cutoff radius was introduced. This suggests that large particles completely dominate the optical behavior of the cloud. For the S cases the system was solved for large, solid particles with an AR value of 1.05 and a RI that ranged from 1.37 to 1.43.

B. Period of 9 December 2001

The second set of observations, also from Kiruna, are from 9 December 2001. The balloon made two ascents and descents through a PSC between 120 and 330 km downwind of Esrange.[25] The PSC was observed between 22 and 26.3 km. Temperatures were below T_{STS} in the lower portion of the cloud that we study here. Embedded within this layer was a narrow layer in which temperatures were 3 K below T_{ICE}. Further details of the observations in the upper cloud can be found in Ref. 25.

The time series subinterval from 78490 to 78870 s of aerosol depolarization, the backscatter coefficient at 532 nm, and the temperature measured by the LABS are shown in Fig. 6(a). Figure 6(b) shows the same time sequence of concentration density as that obtained with the OPC measurement. The optical measurements and data from the OPC suggest that the lower PSC is dominated by STS particles with an embedded ice layer, whereas in the upper part the predominant particles should be NAT.[25]

For this paper only the first part of the chosen time series has been considered to study the type II PSC, which is the only PSC type not present during the 25 January 2000 flight. The time sequence has been divided into three subintervals of $L1$, $Gd1$ and $L2$. In $L1$ and $L2$ PSC particles can be considered as liquid because of their low values of volume depolarization and high aerosol backscatter coefficient value. On the other hand, in $Gd1$ there is a depolarization peak in which the volume and density of large particles suggest that the gondola crossed the ice layer. The same algorithm has been applied in the $L1$, $Gd1$, and $L2$ subintervals assuming particle distributions formed by liquid particles (AR = 1 and RI = 1.53) up to a radius of 0.56 μm, as well as solid particles from 0.56 to 12 μm with variable AR and RI. In this way we calculated the theoretical optical characteristics of PSC particle distributions $\{[\beta_M^p(\mathrm{RI}, \mathrm{AR}, t)]$ and $[\delta_M^p(\mathrm{AR}, \mathrm{RI}, t)]\}$ for each time interval. The two constraints in inequalities (11) and (12) were applied and the results are shown in Fig. 7. The first two panels represent subintervals $L1$ and $L2$. It is evident that the distribution is formed by STS particles and, moreover, a few particles with radii greater than 0.56 μm were spherical (AR close to 1), and with a refractive index that ranged from 1.53 to 1.59. The last panel in Fig. 7 shows the $Gd1$ subinterval. For this situation there are some different particle characteristics that are consistent with Fig. 7:

(1) prolate spheroids with an AR ranging from 1.3 to 1.8 and from RI 1.31 to 1.33,
(2) prolate spheroids with an AR close to 1.35 and a RI of 1.37,
(3) oblate spheroids with a RI from 1.41 to 1.43 and an AR of 0.75, and
(4) oblate spheroids with a RI from 1.47 to 1.59 and an AR that ranged from 0.60 to 0.70.

Case (1) is what was expected on the basis of the qualitative analysis made by Deshler *et al.*[25] as those characteristics correspond to ice particles with a high degree of asphericity. The second and the third cases could represent NAT particles and the different values of RI are probably due to a different state of formation. To satisfy the last case the cloud should

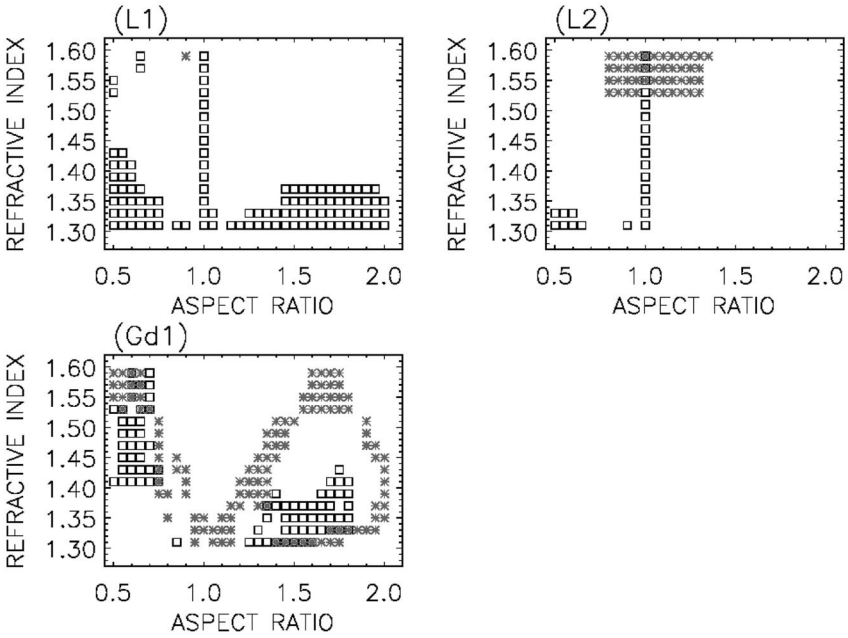

Fig. 7. Kiruna, 9 December 2001. Particle distribution is formed by particles with $R < 0.56$ μm in the liquid phase and particles with $R > 0.56$ μm in the solid phase. For each subinterval the crosses represent pairs of RI and AR that fulfill the backscatter coefficient inequality (11). The open squares represent pairs of RI and AR that satisfy inequality (12) for solid particles.

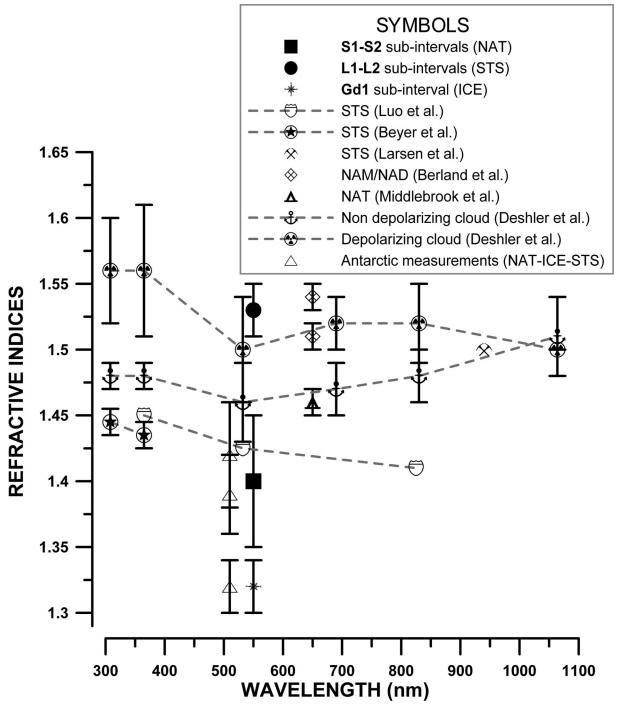

Fig. 8. Index of refraction as a function of wavelength. The indices shown here are the mean values for each defined time subinterval, and the errors represents the variability of the solution. Also depicted are values of refractive indices for depolarizing and nondepolarizing clouds observed in 1996 in the Arctic stratosphere,[26] the results of comparison between OPC and lidar (532 nm) measurements in Antarctica,[27] laboratory measurements at 650 nm for nitric acid monohydrate and NAT,[28,29] laboratory measurements at 308 and 365 nm for a STS,[30] theoretical estimates for STS,[31] and the refractive-index value used to compare chemical and optical measurements at 940 nm.[32] The position on the wavelength axis for measurements at 532 nm are slightly shifted to improve readability of error bars.

have been formed by sulfuric acid tetrahydrate particles of high asphericity. The last three cases are not physically acceptable in the observed conditions, and they should be considered only as mathematical solutions given by the algorithm utilized in this paper.

A summary of the refractive indices inferred from the comparison of theoretical data based on *T*-matrix and scattering measurements at 532 nm on 25 January 2000 and 9 December 2002 is shown in Fig. 8. Figure 8 also shows values of refractive indices for depolarizing and nondepolarizing clouds observed in 1996 in the arctic stratosphere,[26] the results of a comparison between the OPC and the lidar (532-nm) measurements in Antarctica,[27] a laboratory measurement at 650 nm for nitric acid monohydrate and NAT,[28,29] laboratory measurements at 308 and 365 nm for STS,[30] theoretical estimates for STS,[31] and the refractive-index value used to compare chemical and optical measurements at 940 nm.[32] The Lorenz–Lorenz relationship is used along with the Beyer *et al.*[30] constants for ternary solutions to obtain the refractive indices at 308 and 365 nm for STS at a temperature near 190 K.

The values of solid subintervals (*S* and *Gd*) are low with respect to the results inferred by Deshler *et al.*[26] for the depolarizing layer cloud. On the other hand, they are in agreement with the Antarctic measurements of NAT and ice particles published by Adriani *et al.*[27] Liquid subinterval values (*L* and *Ld*) are not fully consistent either with laboratory measurements made by Luo *et al.*[31] or with those found by Deshler *et al.*[26] for a nondepolarizing layer who found those values only for higher wavelengths. In additional research we will concentrate on these discrepancies and their possible solutions.

6. Conclusions

We have proposed a method of analyzing the properties of some chemical and physical particles in the stratosphere for the study of polar stratospheric clouds. During the Comprehensive Investigations of Polar Stratospheric Aerosols campaigns carried out on 25 January 2000 and 9 December 2001 near Kiruna, Sweden, the time series of particle concentration and optical parameters, such as the depolarization and the backscattering ratio, were measured in relation to events of PSCs. We introduced a qualitative analysis of the optical data and the distributions of concentration of the flight of 25 January 2000. Five temporal subintervals were selected when it was possible to make an approximate determination of the presence of various typologies of PSCs by means of their optical parameters. In particular the first and last subintervals are characterized by liquid particles, the second and the third have been described by NAT particles whereas, during the quarter interval, the sonde crossed a layer of the cloud in a phase of solid–liquid transition. Subsequently, a methodology based on the T-matrix theory for simulating a PSC in its interaction with a sounding laser was described. The theoretical values of the optical parameters, such as the aerosol backscatter coefficient and the aerosol depolarization, have been computed as a function of the composition (index of refraction) and shape parameter (aspect ratio) of particles, applying the algorithm to the time series of measured particle size distributions and assuming that those particles had a spheroidal shape and the same phase.

A method that allows us to compare measurement data with theoretical values for each of the five subintervals was developed. We have given the values of aspect ratio and refractive index that correspond to the values of the backscatter coefficient and aerosol depolarization that fulfill the two comparison conditions. The zones of intersection between the two sets of points determine the possible shapes and compositions of the particle.

For the NAT particles in $S1$ and $S2$ subintervals the value of the index of refraction can vary from 1.37 to 1.45 and the AR value is approximately 1.05, which corresponds to a slightly prolate spheroid solid particle. For the liquid particles in $L1$ and $L2$ the mean refractive index is 1.53–1.55 with an aspect ratio close to 1, which can be associated with liquid spherical particles. These results are in agreement with those presented with the quality analysis.

To improve our model we recomputed the optical coefficients assuming a bimodal distribution formed by particles in both a liquid phase and a solid phase. A cutoff radius has been defined to divide the size distribution into two parts. The value of the cutoff radius had been determined by a sensitivity study. In doing this, we fixed the AR and the RI of the particles below the cutoff radius, leaving, as the only unknown variable, the RI and the degree of asphericity of the particles above the cutoff radius. The results obtained by the comparisons with the experimental data show a high dependency of the optical parameters on particles in the solid phase. Better modeling was obtained for those cases in which the optical response of a cloud was not dominated by one side of the size distribution and/or one phase of its constituting particles, namely, for mixed phase clouds. We tested the new model on the data of the 9 December 2001 flight. We processed only the data from the first part of the flight; the algorithm reproduced those data as a possible PSC ice layer with a low RI and a high degree of asphericity in accordance with the above qualitative analysis.

We are grateful to the Centre National d'Etudes Spatiales and the Swedish Space Corporation who supported and permitted the realization of the balloon flights from Esrange, Kiruna, Sweden, during the period from 1998 to 2002. The Comprehensive Investigation of Polar Stratospheric Aerosol project was funded by the Commission of the European Union and the U.S. National Science Foundation (OPP-0095158).

References

1. "WMO Annual report 2001," WMO No. 935 (World Meteorological Organization, Geneva, Switzerland, 2002).
2. A. R. Ravishankara and D. R. Hanson, "Differences in the reactivity of Type I polar stratospheric clouds depending on their phase," J. Geophys. Res. **101** (D2), 3885–3890 (1996).
3. A. I. Carswell, "Lidar measurements of the atmosphere," Can. J. Phys. **61,** 378–395 (1993).
4. E. V. Browell, S. Ismail, A. F. Carter, N. S. Higdon, C. F. Butler, P. A. Robinette, O. B. Toon, M. R. Schoeberl, and A. F. Tuck, "Airborne lidar observations in the wintertime arctic stratosphere: polar stratospheric clouds," Geophys. Res. Lett. **17,** 385–388 (1990).
5. F. Arnold, K. Petzoldt, and E. Reimer, "On the formation and sedimentation of stratospheric nitric acid aerosols: implications for polar ozone destruction," Geophys. Res. Lett. **19,** 677–680 (1992).
6. K. S. Carslaw, B. P. Luo, S. L. Clegg, T. Peter, P. Brimblecombe, and P. J. Crutzen, "Stratospheric aerosol growth and HNO_3 gas phase depletion from coupled HNO_3 and water uptake by liquid particles," Geophys. Res. Lett. **21,** 2479–2482 (1994).
7. A. Tabazadeh, R. P. Turco, K. Drdla, M. Z. Jacobson, and O. B. Toon, "A study of Type I polar stratospheric cloud formation," Geophys. Res. Lett. **21,** 1619–1622 (1994).
8. P. J. Crutzen and F. Arnold, "Nitric acid cloud formation in the cold Antarctic stratosphere: a major cause for the springtime ozone hole," Nature **324,** 651–655 (1986).
9. O. B. Toon, P. Hamill, R. P. Turco, and J. Pinto, "Condensation of HNO_3 and HCl in the winter polar stratosphere," Geophys. Res. Lett. **13,** 1284–1287 (1986).
10. D. Hanson and K. Mauersberger, "Laboratory studies of the nitric acid tridydrate: implications for the South polar stratosphere," Geophys. Res. Lett. **15,** 855–858 (1988).
11. C. Voigt, J. Schreiner, A. Kohlmann, P. Zink, K. Mauersberger, N. Larsen, T. Deshler, C. Kröger, J. Rosen, A. Adriani, F. Cairo, G. Di Donfrancesco, M. Viterbini, J. Ovarlez, H. Ovarlez, C. David, and A. Dörnbrack, "Nitric acid trihydrate in polar stratospheric clouds," Science **290,** 1756–1758 (2000).
12. M. I. Mishchenko and L. D. Travis, "T-matrix computations of light scattering by large spheroidal particles," Opt. Commun. **109,** 16–21 (1994).

13. M. I. Mishchenko, J. W. Hovenier, and L. D. Travis, eds., *Light Scattering by Nonspherical Particles: Theory, Measurements, and Applications* (Academic, San Diego, Calif., 1999), pp. 3–27.
14. J. R. Bottiger, E. S. Fry, and R. C. Thompson, "Phase matrix measurements for electromagnetic scattering by sphere aggregates," in *Light Scattering by Irregularly Shaped Particles*, D. W. Schuerman, ed. (Plenum, New York, 1980), pp. 283–290.
15. A. Mugnai and W. J. Wiscombe, "Scattering from nonspherical Chebyshev particles. I: Cross sections, single-scattering albedo, asymmetry factor, and backscattered fraction," Appl. Opt. **25,** 1235–1244 (1986).
16. P. C. Waterman, "Matrix formulation of electromagnetic scattering," Proc. IEEE **53,** 805–812 (1965).
17. M. I. Mishchenko and L. D. Travis, "Capabilities and limitations of a current FORTRAN implementation of the *T*-matrix method for randomly oriented, rotationally symmetric scatterers," J. Quant. Spectrosc. Radiat. Transfer **60,** 309–324 (1998).
18. T. Deshler and S. J. Oltmans, "Vertical profiles of volcanic aerosol and polar stratospheric clouds above Kiruna, Sweden: winter 1993 and 1995," J. Atmos. Chem. **30,** 11–23 (1998).
19. A. Adriani, F. Cairo, S. Mandolini, G. Di Donfrancesco, T. Deshler, and B. Nardi, "A new joint balloon-borne experiment to study polar stratospheric clouds: laser backscattersonde and optical particle counter," in *Atmospheric Ozone, Proceedings of the XVIII Quadrennial Ozone Symposium*, Vol. 2, R. D. Bojkov and G. Visconti, eds. (Edigrafital for Parco Scientifico e Tecnologico d'Abruzzo, 1998), pp. 879–882.
20. J. M. Rosen and N. T. Kjome, "Backscattersonde: a new instrument for atmospheric aerosol research," Appl. Opt. **30,** 1552–1561 (1991).
21. T. Deshler, B. J. Johnson, W. R. Rozier, and D. J. Hofmann, "Balloonborne measurements of the Pinatubo aerosol size distribution and volatility at Laramie, Wyoming during the summer of 1991," Geophys. Res. Lett. **19,** 199–202 (1992).
22. A. T. Young, "Rayleigh scattering," Appl. Opt. **20,** 533–535 (1981).
23. J. Biele, A. Tsias, B. P. Luo, K. S. Carslaw, R. Neuber, G. Beyerle, and T. Peter, "Nonequilibrium coexistence of solid and liquid particles in Arctic stratospheric clouds," J. Geophys. Res. **106** (D19), 22991–23008 (2001).
24. G. P. Gobbi, G. Di Donfrancesco, and A. Adriani, "Physical properties of stratospheric clouds during the Antarctic winter of 1995," J. Geophys. Res. **103** (D9), 10859–10874 (1998).
25. T. Deshler, N. Larsen, C. Weissner, J. Schreiner, K. Mauersberger, F. Cairo, A. Adriani, G. Di Donfrancesco, J. Ovarlez, H. Ovarlez, U. Blum, K. H. Fricke, and A. Dörnbrack, "Large nitric acid particles at the top of an Arctic stratospheric cloud," J. Geophys. Res. **108** (D16), 4517, doi:10.1029/2003JD003479 (2003).
26. T. Deshler, B. Nardi, A. Adriani, F. Cairo, G. Hansen, F. Fierli, A. Hauchecorne, and L. Pulvirenti, "Determining the index of refraction of polar stratospheric clouds above Andoya (69 °N) by combining size-resolved concentration and optical scattering measurements," J. Geophys. Res. **105** (D3), 3943–3954 (2000).
27. A. Adriani, T. Deshler, G. Di Donfrancesco, and G. P. Gobbi, "Polar stratospheric clouds and volcanic aerosol during spring 1992 over McMurdo Station, Antarctica: lidar and particle counter comparisons," J. Geophys. Res. **100** (D12), 25877–25898 (1995).
28. B. S. Berland, D. R. Haynes, K. L. Foster, M. A. Tolbert, S. M. George, and O. B. Toon, "Refractive indices of amorphous and crystalline HNO_3/H_2O films representative of Polar Stratospheric Clouds," J. Phys. Chem. **98,** 4358–4364 (1994).
29. A. M. Middlebrook, B. S. Berland, S. M. George, M. A. Tolbert, and O. B. Toon, "Real refractive indices of infrared-characterized nitric-acid/ice films: implications for optical measurements of polar stratospheric clouds," J. Geophys. Res. **99** (D12), 25655–25666 (1994).
30. K. D. Beyer, A. R. Ravishankara, and E. R. Lovejoy, "Measurements of UV refractive indices and densities of $H_2S_2O_4/H_2O$ and $H_2S_2O_4/HNO_3/H_2O$ solutions," J. Geophys. Res. **101** (D9), 14519–14524 (1996).
31. B. Luo, U. K. Krieger, and T. Peter, "Densities and refractive indices of $H_2SO_4/HNO_3/H_2O$ solutions to stratospheric temperatures," Geophys. Res. Lett. **23,** 3707–3710 (1996).
32. N. Larsen, I. S. Mikkelsen, B. M. Knudsen, J. Schreiner, C. Voigt, K. Mauersberger, J. M. Rosen, and N. T. Kjome, "Comparison of chemical and optical *in situ* measurements of polar stratospheric cloud particles," J. Geophys. Res. **105** (D1), 1491–1502 (2000).